Supplementary Information

## RNAi revised — target mRNA-dependent enhancement of gene silencing

Simon Dornseifer[1], Sarah Willkomm[1], Rosel Kretschmer-Kazemi Far[1], Janine Liebschwager[1], Foteini Beltsiou[1], Kirsten Frank[1], Sandra D. Laufer[1§], Thomas Martinetz[2], Georg Sczakiel[1], Jens Christian Claussen[2#] and Tobias Restle[1]*

[1]Institute of Molecular Medicine and [2]Institute for Neuro- and Bioinformatics, University of Lübeck, 23538 Lübeck, Germany

present address: §Hamburg Centre for Experimental Therapy Research (HEXT), Universitätsklinikum Hamburg-Eppendorf, Martinistr. 52, 20246 Hamburg and #Systems Biology Lab, Jacobs University Bremen, Campus Ring 1, 28759 Bremen, Germany

*To whom correspondence should be addressed. Tel: 0049-451-500-2745; Fax: 0049-451-2729; Email: restle@imm.uni-luebeck.de
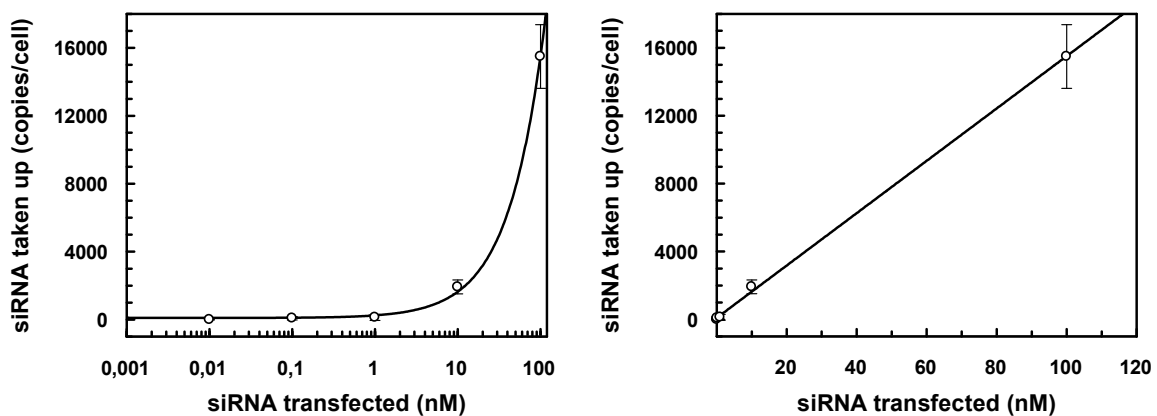
Supplementary Figure S1: Correlation between siRNA transfected and cellular uptake of siRNA. Twenty four hours prior to transfection, HTO cells were seeded into 12 well plates at about 4 x 10^5 cells/well. siR206 was transfected at different concentrations with 10 µg/ml LF2000. Twenty four hours past transfection the amount of siRNA taken up by the cells was determined applying a liquid hybridisation assay. For experimental details see Materials and Methods. The graph shows one representative experiment in duplicates. Logarithmic scale to the left and linear scale to the right.
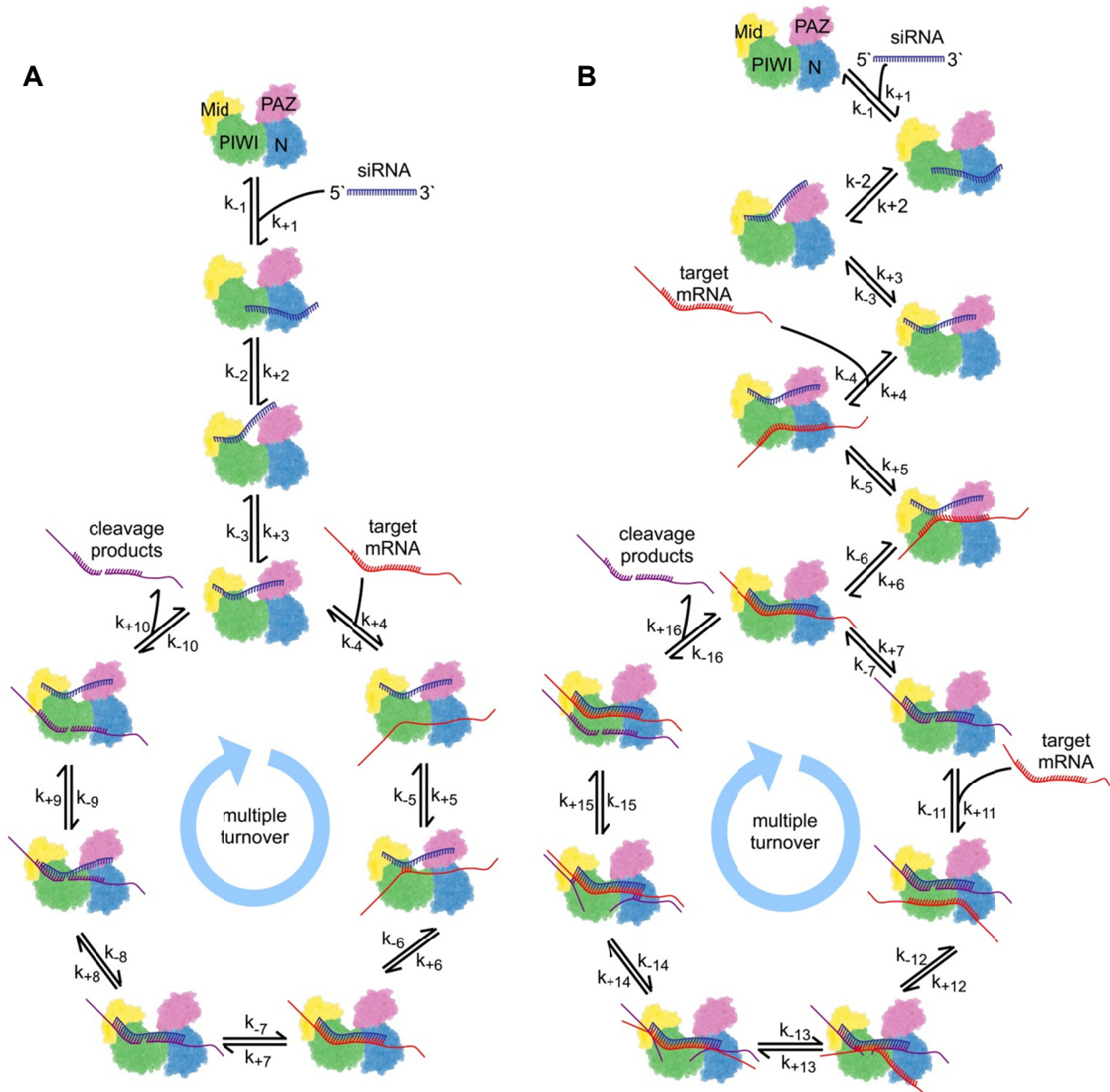
Supplementary Figure S2: Illustration of the two proposed models of RNAi in mammalian cells. (A) Dissociative and (B) associative model. The illustrations are closely based on Scheme 1 of (1). Ago2 is represented as electron density cloud with the four domains N, PAZ, Mid, and PIWI coloured individually in blue, magenta, yellow and green, respectively. RNAs are indicated by lines and colour blue, red or purple for guide, target or product strands. The relative spatial positions of protein and RNA substrates are indicated and formation of Watson-Crick base pairs is illustrated by short connecting lines between RNA strands. For both models the cycle starts with binary complex formation between ss guide RNA and Ago2 followed by association of a target RNA leading to a catalytically active ternary complex composed of Ago2, guide and target RNA. Note: potential co-factors, passenger strand cleavage and release during binary complex formation are omitted for clarity but essentially, the proposed pathway also holds true for ds siRNA. Next, the target RNA gets cleaved as illustrated by the colour change from red to purple. Subsequently, the two models diverge. In the dissociative model, the products dissociate, new target RNA binds to the binary complex of Ago and guide and the catalytic cycle starts over. In the associative model, new target binds to a ternary Ago2-guide-product complex forming a quaternary intermediate followed by replacement of the product fragments eventually leading to a catalytically active ternary complex and likewise the cycle starts over. Corresponding rate equations 1-10 (dissociative model) and 1-7 and 11-16 (associative model) are given below (Supplementary Equations 1). The rate constants for each individual step (i.e. k_{+1} - k_{-16}) are listed in Supplementary Table S1.
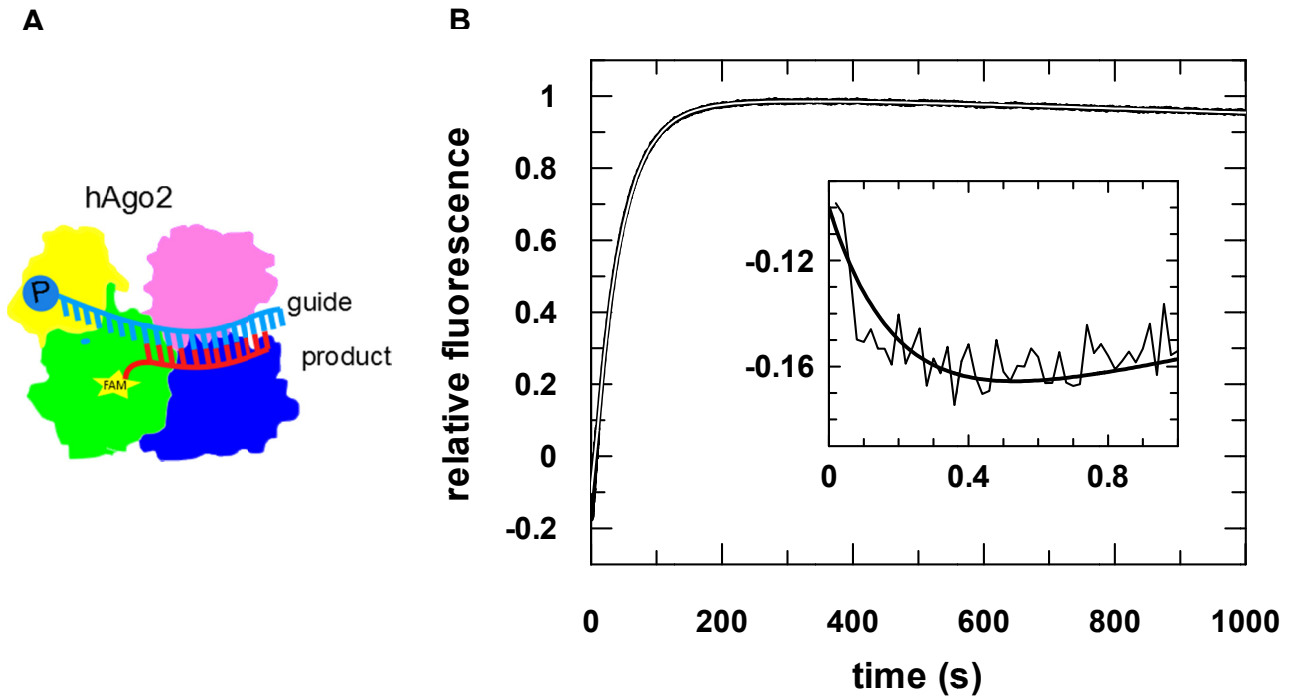
Supplementary Figure 3: Dissociation of product-like RNA from ternary complexes. A) Schematic representation of a hAgo2/guide/product ternary complex. The product RNA (5'-uag agg uac gug-3') carries a FAM label at its 3'-end and is fully complementary to guide nucleotides 8 – 19. B) Preassembled ternary complexes comprising 500 nM hAgo2, 20 nM guide (s2b) and 20 nM product RNA (as2b_short[FAM]) were rapidly mixed with 2 μM unlabeled target strand (as2b). A representative stopped-flow graph is shown. The inset shows the reaction on a shorter time scale. Data could be fitted best to a triple exponential equation yielding the following rate constants: k_1: 5.2 (± 0.1) s^{-1}, k_2: 0.03 (± 8 x 10^{-5}) s^{-1} and k_3: 0.006 (± 0.0005) s^{-1}.
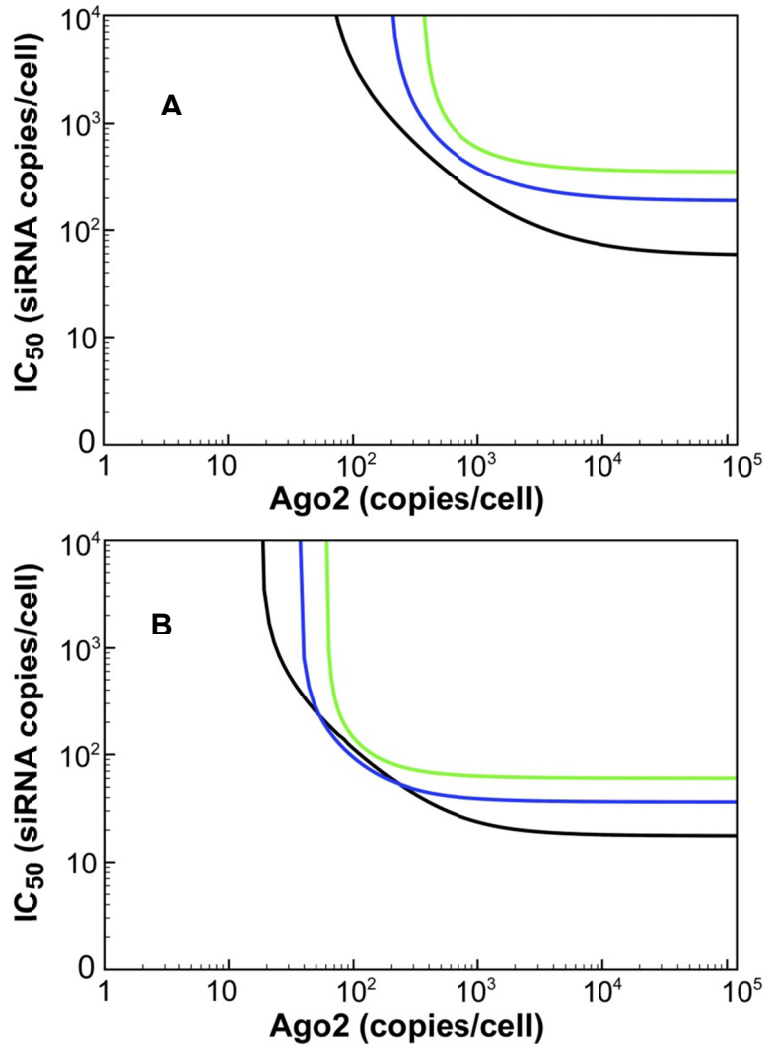
Supplementary Figure S4: Relation between Ago2 concentration and IC$_{50}$. (A) For the dissociative and (B) the associative models, logarithmically-scaled IC$_{50}$, the half maximal inhibitory siRNA concentration after 24 h of knockdown, is plotted against logarithmically-scaled Ago2 concentration. Basal target concentrations are 1000 (black), 5000 (blue) and 10,000 (green lines) copies per cell, respectively.
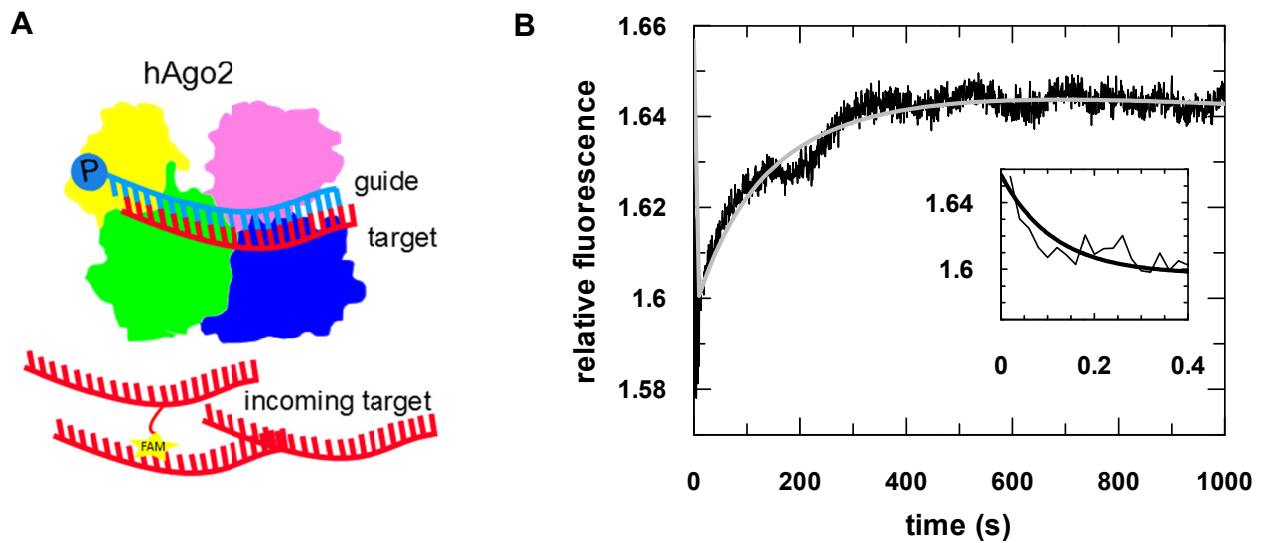
Supplementary Figure S5: Target binding to preformed ternary complexes. A) Schematic representation of the experimental setup; association of target RNAs with ternary hAgo2/guide/target complexes. A FAM fluorophore is linked to nucleotide 14 of the incoming target strand counted from the 5'-end. B) Ternary complexes comprising 600 nM hAgo2, 20 nM guide (s2b) and 30 nM target RNA (OH-as2b) were rapidly mixed with 90 nM free target RNA (OH-as2b^{FAM}). A representative stopped-flow graph is shown. Data could be fitted best using a triple exponential equation yielding the following rate constants: $k_{1\_obs} = 8.9 \pm 0.5$ s^{-1}; $k_2 = 0.012 \pm 0.0008$ s^{-1}; $k_3 = 0.0045 \pm 0.0003$ s^{-1}.
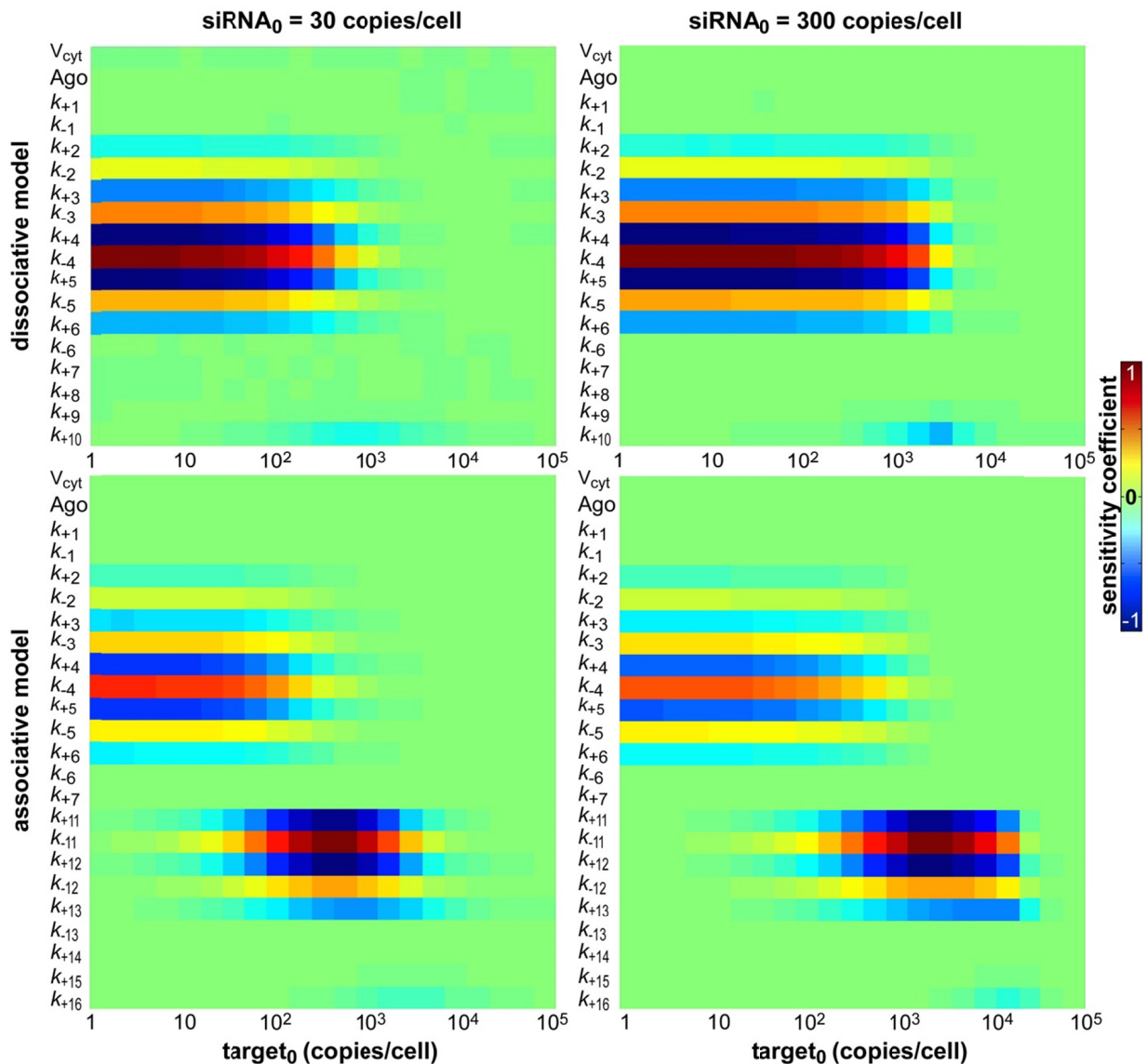
Supplementary Figure S6: Sensitivity plot of time-resolved target knockdown. The sensitivity of target knock-down efficacy to changes in model parameters S_i (y axis) is provided for varying target concentrations (x axis). Investigated parameters S_i are kinetic rate constants k_{+1} to k_{+16} and k_{-1} to k_{-13} (Supplementary Table S1), initial concentration of Ago, as well as, cytoplasm volume V_{cyt}. Sensitivity is shown for the dissociative (upper row) and the associative (lower row) model for two different siRNA concentrations; 30 (left column) and 300 (right column) copies/cell. The colour illustrates sensitivities; dark red (sensitivity coefficient close to 1; decrease of parameter value leads to high target knock-down efficacy) and dark blue (sensitivity coefficients close to -1; increase of parameter value leads to high target knock-down efficacy) indicate high sensitivity and green (sensitivity coefficient close to 0) indicates that a change of parameters has no considerable effect on target knock-down efficacy. Details are given below (sensitivity analysis).

6
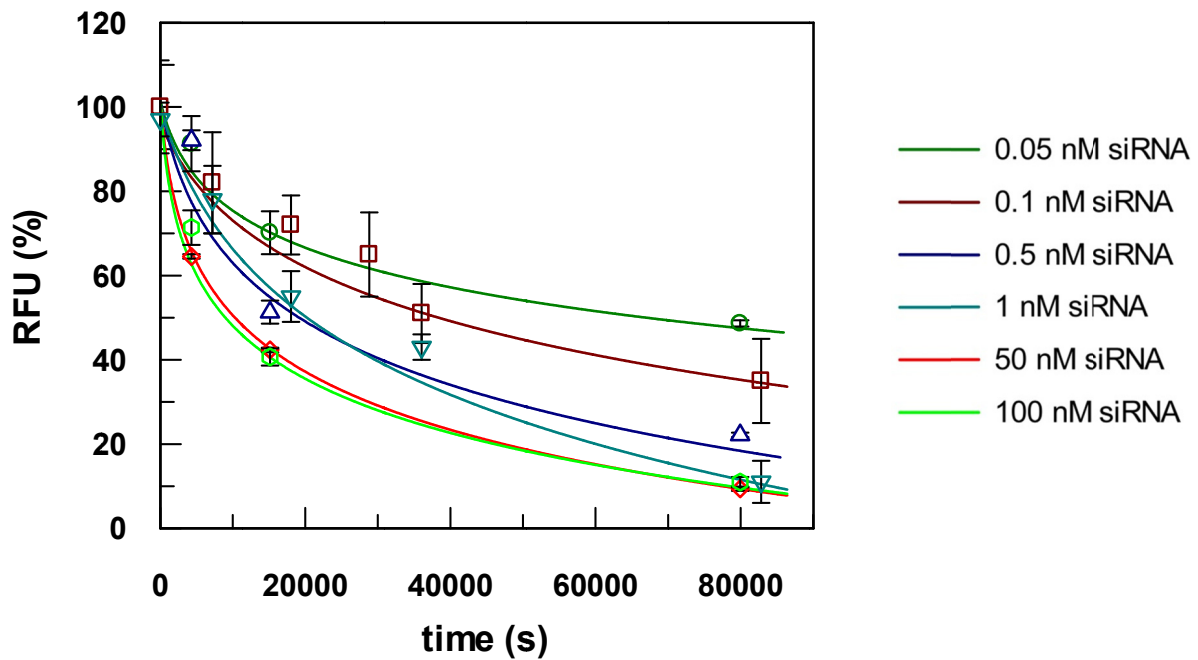
Supplementary Figure S7: Calculation of $t_{1/2}$ values of knock-down of luciferase reporter gene activity after LF2000-mediated transfection of different amounts of siR206. HTOL cells were transfected for 1 h with 0.05, 0.1, 0.5, 1, 50 and 100 nM siR206 or a scrambled siRNA (sisc: 5'-CGAACUCACUGGUCUGACCtt-3'). After the time intervals given luminescence was measured in a microplate reader. Luminescence was normalised to cell viability (FDA) to account for cell loss due to cytotoxicity or washing procedures, and to the scrambled siRNA control to account for potential fluctuations in reporter signal caused by the transfection procedure. For $t_{1/2}$ calculation the experimental data were fitted to y = a log(t) + b, where t is time in s and y is RFU in %, using the least-square fit routine of the optim package of GNU Octave. The corresponding $t_{1/2}$ values are: 0.05 nM = 19 (± 2.5), 0.1 nM = 10.6 (± 2.4), 0.5 nM = 6.7 (± 0.3), 1 nM = 5.6 (± 0.4), 50 nM = 3.5 (± 0.2) and 100 nM siR206 = 2.9 (± 0.25) h. The data are an average of at least two independent experiments. SD is given by error bars.
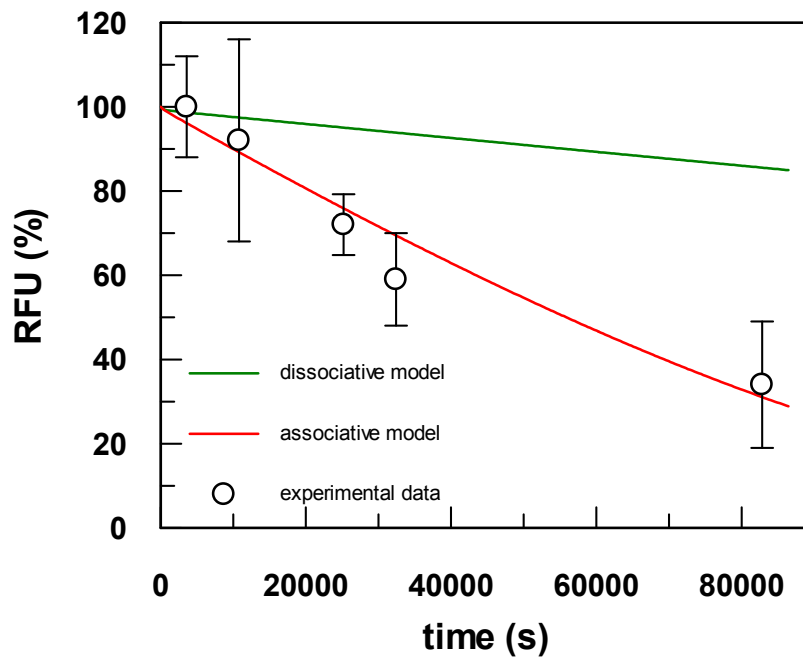
Supplementary Figure S8: Comparison of simulated and experimentally determined time resolved siRNA-mediated target knockdown. HTO cells were transfected for 4 h with 100 ng/well pTRE2hyg-luc plasmid in 96 well plates. This concentration of plasmid in the LF2000 transfection mix translates into 560 (± 107) luciferase mRNA copies per cell as determined by qPCR. 24 h post plasmid transfection cells were again transfected with 0.75 nM siR206 or a scrambled siRNA control (sisc: see Supplementary Figure S7) for 1 h. 0.75 nM siRNA in the transfection mix translates into 470 copies of bioavailable siR206 per cell (Supplementary Figure S1). At time intervals given luminescence was measured in a microplate reader. Luminescence was normalised to cell viability (FDA) to account for cell loss due to cytotoxicity or washing procedures, and to the scrambled siRNA control to account for potential fluctuations in reporter signal caused by the transfection procedure. Measurements were performed in quadruplicate. SD is given by error bars. Simulation results of the dissociative (green line) and associative (red line) model at 560 and 470 copies/cell of target and siRNA, respectively, are shown for comparison.

A

seed-matched competitor RNA

B
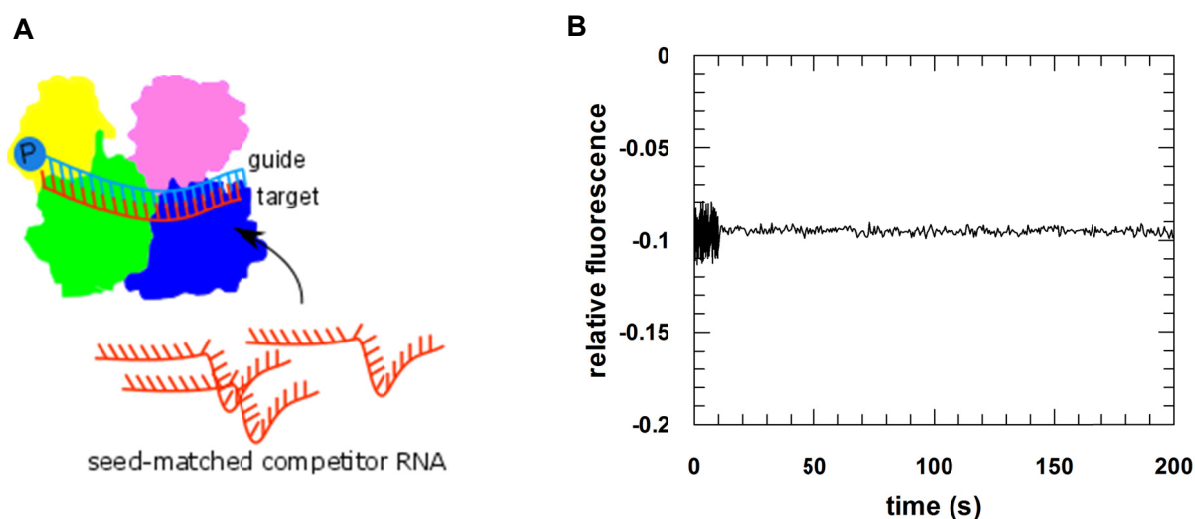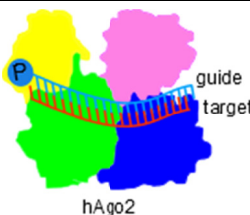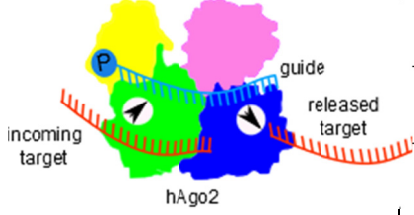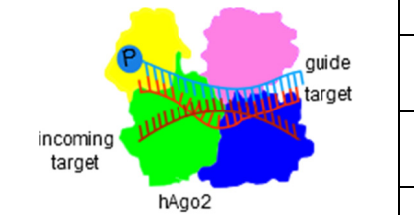
Supplementary Figure S9: Competition of ternary complexes with a seed matching trap oligo. A) Schematic representation of the experimental setup. The competitor RNA supposed to trap the binary complex after dissociation of the target displays complementarity to the seed region of the guide strand. B) Preassembled ternary complexes comprising 500 nM hAgo2, 20 nM guide (as2b^{FAM}) and 40 nM fully complementary target RNA (s2b) were rapidly mixed with 2 µM unlabeled target strand (s2bmm-3′) displaying complementarity to the seed region of the guide strand. Oligonucleotide sequences are given in (1). A representative stopped-flow graph is shown. As indicated by the flat line no competition could be observed.

A

non-seed-matched competitor RNA

B
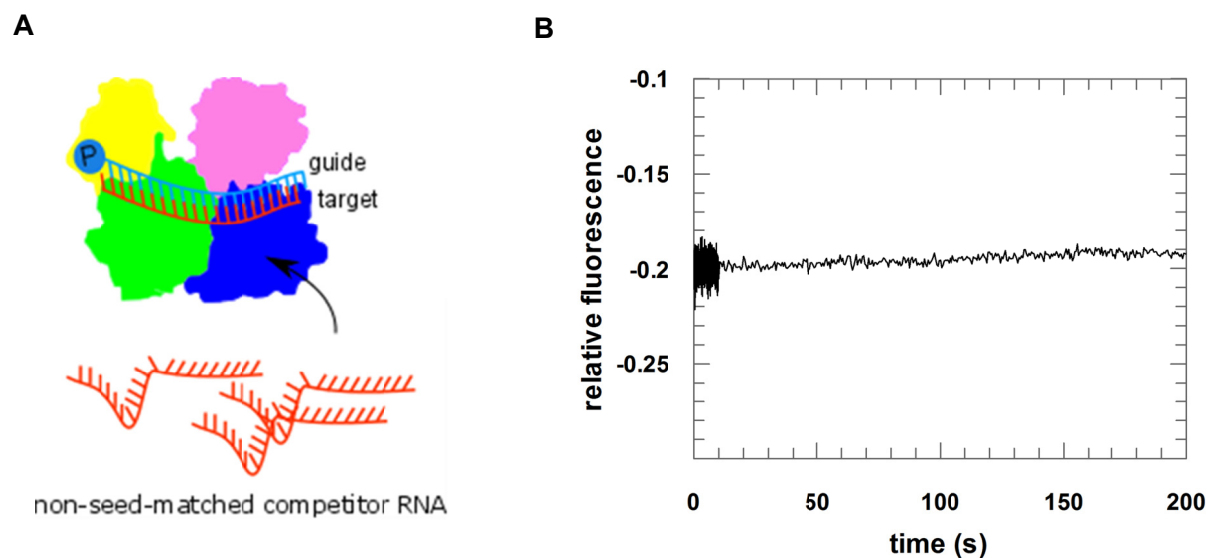
Supplementary Figure S10: Competition of ternary complexes with a trap matching the 3'-half of the guide strand. A) Schematic representation of the experimental setup. The competitor RNA supposed to trap the binary complex after dissociation of the target displays complementarity to the 3'-half of the guide strand. B) Preassembled ternary complexes comprising 500 nM hAgo2, 20 nM guide (as2b^{FAM}) and 40 nM fully complementary target RNA (s2b) were rapidly mixed with 2 µM unlabeled target strand (s2bmm-5′) displaying complementarity to the 3'-half of the guide strand. Oligonucleotide sequences are given in (1). A representative stopped-flow graph is shown. As indicated by the flat line no competition could be observed.

9

Illustration		Reaction step	k	Dis	As	Value	Unit
siRNA binding		binary complex formation 1	k_{+1}	+	+	0.6×10^8	$M^{-1}s^{-1}$
			k_{-1}	+	+	6.2	s^{-1}
		binary complex formation 2	k_{+2}	+	+	0.3	s^{-1}
			k_{-2}	+	+	0.2	s^{-1}
		binary complex formation 3	k_{+3}	+	+	0.01	s^{-1}
			k_{-3}	+	+	0.007	s^{-1}
Target binding		ternary complex formation 1	k_{+4}	+	+	3.2×10^8	$M^{-1}s^{-1}$
			k_{-4}	+	+	2	s^{-1}
		ternary complex formation 2	k_{+5}	+	+	0.01	s^{-1}
			k_{-5}	+	+	0.002	s^{-1}
		ternary complex formation 3	k_{+6}	+	+	0.003	s^{-1}
			k_{-6}	+	+	0.0002	s^{-1}
		target cleavage	k_{+7}	+	+	10	s^{-1}
			k_{-7}	+	+	-	s^{-1}
Dissociative path		product release 1	k_{+8}	+	-	1.2	s^{-1}
			k_{-8}	+	-	-	s^{-1}
		product release 2	k_{+9}	+	-	0.002	s^{-1}
			k_{-9}	+	-	-	s^{-1}
		product release 3	k_{+10}	+	-	0.0002	s^{-1}
			k_{-10}	+	-	-	s^{-1}
Associative path		quaternary complex formation 1	k_{+11}	-	+	3.2×10^8	$M^{-1}s^{-1}$
			k_{-11}	-	+	2	s^{-1}
		quaternary complex formation 2	k_{+12}	-	+	0.01	s^{-1}
			k_{-12}	-	+	0.002	s^{-1}
		quaternary complex formation 3	k_{+13}	-	+	0.003	s^{-1}
			k_{-13}	-	+	0.0002	s^{-1}
		product release 1	k_{+14}	-	+	5	s^{-1}
			k_{-14}	-	+	-	s^{-1}
		product release 2	k_{+15}	-	+	0.03	s^{-1}
			k_{-15}	-	+	-	s^{-1}
		product release 3	k_{+16}	-	+	0.006	s^{-1}
			k_{-16}	-	+	-	s^{-1}

Supplementary Table S1: Kinetic rate constants used for modelling RNAi. For each elementary reaction step, a forward and backward rate constant pair is provided. Columns 'Dis' and 'As' indicate the parameters used in either the dissociative or associative model. If both, forward and backward rate constants are provided, reaction steps are modelled as reversible. Else, a reaction step is modelled as quasi-irreversible like for example in case of the target cleavage step. Association and dissociation rate constants for binary and ternary hAgo2/RNA complexes have been reported previously (1). Association of quaternary complex formation is shown in Supplementary Figure S5. For k_{-11} - k_{-13} rate constants of dissociation of ternary complexes (k_{-4} - k_{-6}) were used as a basis. Dissociation of product-like RNA from ternary complexes in the presence of un-cleaved target is shown in Supplementary Figure S3. Currently, the pre-steady state cleavage rate of hAgo is not available. Instead, we used the value of ~10 s^{-1} determined for HIV-1 reverse transcriptase (2) which comprises a conserved RNase H fold and is the only enzyme where the pre-steady state rate constant for RNA cleavage has been measured. The cartoons to the left illustrate the corresponding protein/nucleic acid complex.

parameter	S	C	value	unit	ref.
cytoplasm volume	V_{cyto}	-	2.5×10^{-12}	l	(3-7)
initial siRNA	$[S]_0$	V_{cyto}	30 4.98×10^{-5}	copies/cell nM	sample value
basal hAgo2 level	$[A]_0$	V_{cyto}	200,000 132.84	copies/cell nM	(8,9)
basal target mRNA level	$[T]_0$	V_{cyto}	1−10,000 6×10^{-5} −67	copies/cell nM	(10)
target degradation rate	k_{deg}	-	6.40×10^{-5}	s^{-1}	(11,12)
target synthesis rate	v_{synth}	-	1.27×10^{-14}	M s^{-1}	(10)

Supplementary Table S2: Reaction compartment volume and species concentrations used for modelling. Column 'S' provides the parameters' symbols. In case of concentration, column 'C' indicates the compartment for which it is given. Calculated from (9), a human cell comprises ~ 1.4×10^5 to 1.7×10^5 Argonautes per cell, where Ago2 is the most abundant of the four Ago-subtypes. According to own measurements, there are ~ 2.5×10^5 copies Ago2 per human cell (13). The basal target mRNA level and initial siRNA concentrations are varied depending on model objective or modelled experimental set up. Physiological mRNA level can vary between 1 and 10,000 copies per human cell (10). Small RNAs involved in RNAi occur in 5 - 500 copies per human cell (14). The minimal number of siRNA molecules (siR206) per cell necessary to trigger half maximal luciferase reporter target knockdown has been determined by microinjection to be of less than 20 copies (15,16).

Kinetic Modelling of RNAi

In this study the RNAi process in mammalian cells is formally described by a network of elementary reactions. Their biochemical rate equations connect experimentally derived *in vitro* reaction rate constants with physiological concentrations of reactants and cell compartment volumes. The reaction mechanism is encoded in the reactions' rate laws, its parameters (Supplementary Table S2), and the way the reactions are linked to one another in the two alternative metabolic pathways (Supplementary Figure S2). The reactions for the dissociative model translate in reaction equations (1) - (10).

$$A + S \underset{k_{-1}}{\overset{k_{+1}}{\rightleftharpoons}} AS \tag{1}$$

$$AS \underset{k_{-2}}{\overset{k_{+2}}{\rightleftharpoons}} AS^{\dagger} \tag{2}$$

$$AS^{\dagger} \underset{k_{-3}}{\overset{k_{+3}}{\rightleftharpoons}} AS^{\ddagger} \tag{3}$$

$$AS^{\ddagger} + T \underset{k_{-4}}{\overset{k_{+4}}{\rightleftharpoons}} AST \tag{4}$$

$$AST \underset{k_{-5}}{\overset{k_{+5}}{\rightleftharpoons}} AST^{\dagger} \tag{5}$$

$$AST^{\dagger} \underset{k_{-6}}{\overset{k_{+6}}{\rightleftharpoons}} AST^{\ddagger} \tag{6}$$

$$AST^{\ddagger} \underset{k_{-7}}{\overset{k_{+7}}{\rightleftharpoons}} ASQ \tag{7}$$

$$ASQ \underset{k_{-8}}{\overset{k_{+8}}{\rightleftharpoons}} ASQ^{\dagger} \tag{8}$$

$$ASQ^{\dagger} \underset{k_{-9}}{\overset{k_{+9}}{\rightleftharpoons}} ASQ^{\ddagger} \tag{9}$$

$$ASQ^{\ddagger} \underset{k_{-10}}{\overset{k_{+10}}{\rightleftharpoons}} AS^{\ddagger} + Q \tag{10}$$

$$ASQ^{\ddagger} + T \underset{k_{-11}}{\overset{k_{+11}}{\rightleftharpoons}} ASQT \tag{11}$$

$$ASQT \underset{k_{-12}}{\overset{k_{+12}}{\rightleftharpoons}} ASQT^{\dagger} \tag{12}$$

$$ASQT^{\dagger} \underset{k_{-13}}{\overset{k_{+13}}{\rightleftharpoons}} ASQT^{\ddagger} \tag{13}$$

$$ASQT^{\ddagger} \underset{k_{-14}}{\overset{k_{+14}}{\rightleftharpoons}} ASTQ \tag{14}$$

$$ASTQ \underset{k_{-15}}{\overset{k_{+15}}{\rightleftharpoons}} ASTQ^{\dagger} \tag{15}$$

$$ASTQ^{\dagger} \underset{k_{-16}}{\overset{k_{+16}}{\rightleftharpoons}} AST^{\ddagger} + Q \tag{16}$$
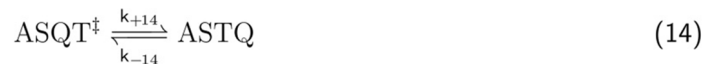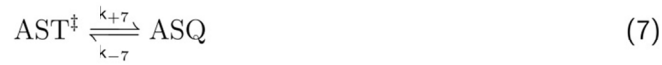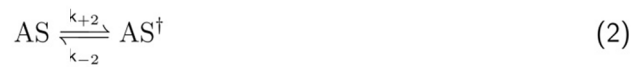
Supplementary Equations 1.

Both models share reactions (1) - (7). However, the dissociative model's reactions (8) - (10) are replaced by reactions (11) - (16) in case of the associative model. Molecular entities are abbreviated as follows: A (Ago), S (ss siRNA or guide RNA), T (target mRNA) and Q (product fragments, resulting from cleavage of T). To distinguish structural states of the system that otherwise have the same composition, dagger (†) and double dagger (‡) symbols may be used. For instance, AST, AST†, and AST‡ are all ternary hAgo2/guide/target complexes which differ solely in their structural conformations.

Time Course Simulations

Mathematically, a network of biochemical reactions can be described by a set of ordinary differential equations (ODEs). Analogous to reactions (1) - (10), the system of ODEs for the dissociative model is defined by equation (17) - (29). All rate laws of these elementary reactions are modelled as mass action whereas catalytic step (7) and the three steps of product release (8) - (10) are considered quasi-irreversible in accordance with their rate constants (Supplementary Equations 1 and Supplementary Table S1).

$$\frac{\mathrm{d}[A]}{\mathrm{d}t} = k_{-1}[AS] - k_{+1}[A][S] \tag{17}$$

$$\frac{\mathrm{d}[S]}{\mathrm{d}t} = k_{-1}[AS] - k_{+1}[A][S] \tag{18}$$

$$\frac{\mathrm{d}[AS]}{\mathrm{d}t} = k_{+1}[A][S] + k_{-2}[AS^\dagger] - k_{-1}[AS] - k_{+2}[AS] \tag{19}$$

$$\frac{\mathrm{d}[AS^\dagger]}{\mathrm{d}t} = k_{+2}[AS] + k_{-3}[AS^\ddagger] - k_{-2}[AS^\dagger] - k_{+3}[AS] \tag{20}$$

$$\frac{\mathrm{d}[AS^\ddagger]}{\mathrm{d}t} = k_{+3}[AS^\dagger] + k_{-4}[AST] + k_{+10}[ASQ^\ddagger] - k_{-3}[AS^\ddagger] - k_{+4}[AS^\ddagger][T] \tag{21}$$

$$\frac{\mathrm{d}[T]}{\mathrm{d}t} = k_{-4}[AST] - k_{+4}[AS^\ddagger][T] \tag{22}$$

$$\frac{\mathrm{d}[AST]}{\mathrm{d}t} = k_{+4}[AS^\ddagger][T] + k_{-5}[AST^\dagger] - k_{-4}[AST][T] - k_{+5}[AST] \tag{23}$$

$$\frac{\mathrm{d}[AST^\dagger]}{\mathrm{d}t} = k_{+5}[AST] + k_{-6}[AST^\ddagger] - k_{-5}[AST^\dagger][T] - k_{+6}[AST] \tag{24}$$

$$\frac{\mathrm{d}[AST^\ddagger]}{\mathrm{d}t} = k_{+6}[AST^\dagger] - k_{-6}[AST^\ddagger][T] - k_{+7}[AST] \tag{25}$$

$$\frac{\mathrm{d}[ASQ]}{\mathrm{d}t} = k_{+7}[AST^\ddagger] - k_{+8}[ASQ] \tag{26}$$

$$\frac{\mathrm{d}[ASQ^\dagger]}{\mathrm{d}t} = k_{+8}[ASQ] - k_{+9}[ASQ] \tag{27}$$

$$\frac{\mathrm{d}[ASQ^\ddagger]}{\mathrm{d}t} = k_{+9}[ASQ^\dagger] - k_{+10}[ASQ] \tag{28}$$

$$\frac{\mathrm{d}[Q]}{\mathrm{d}t} = k_{+10}[ASQ] \tag{29}$$

Supplementary Equations 2.

13

The system of ODEs for the associative model is defined as equation (30) - (45), where all rate laws are modelled as mass action. Catalytic step (7) and the three steps of associative product release (14) - (16) are considered quasi-irreversible in accordance with their rate constants (Supplementary Equations 1 and Supplementary Table S1).

$$\frac{\mathrm{d}[A]}{\mathrm{d}t} = k_{-1}[AS] - k_{+1}[A][S] \tag{30}$$

$$\frac{\mathrm{d}[S]}{\mathrm{d}t} = k_{-1}[AS] - k_{+1}[A][S] \tag{31}$$

$$\frac{\mathrm{d}[AS]}{\mathrm{d}t} = k_{+1}[A][S] + k_{-2}[AS^\dagger] - k_{-1}[AS] - k_{+2}[AS] \tag{32}$$

$$\frac{\mathrm{d}[AS^\dagger]}{\mathrm{d}t} = k_{+2}[AS] + k_{-3}[AS^\ddagger] - k_{-2}[AS^\dagger] - k_{+3}[AS] \tag{33}$$

$$\frac{\mathrm{d}[AS^\ddagger]}{\mathrm{d}t} = k_{+3}[AS^\dagger] + k_{-4}[AST] - k_{-3}[AS^\ddagger] - k_{+4}[AS^\ddagger][T] \tag{34}$$

$$\frac{\mathrm{d}[T]}{\mathrm{d}t} = k_{-4}[AST] + k_{-11}[ASQT] - k_{+4}[AS^\ddagger][T] - k_{+11}[ASQ][T] \tag{35}$$

$$\frac{\mathrm{d}[AST]}{\mathrm{d}t} = k_{+4}[AS^\ddagger][T] + k_{-5}[AST^\dagger] - k_{-4}[AST] - k_{+5}[AST] \tag{36}$$

$$\frac{\mathrm{d}[AST^\dagger]}{\mathrm{d}t} = k_{+5}[AST] + k_{-6}[AST^\ddagger] - k_{-5}[AST^\dagger] - k_{+6}[AST] \tag{37}$$

$$\frac{\mathrm{d}[AST^\ddagger]}{\mathrm{d}t} = k_{+6}[AST^\dagger] + k_{+16}[ASTQ^\ddagger] - k_{-6}[AST^\ddagger][T] - k_{+7}[AST] \tag{38}$$

$$\frac{\mathrm{d}[ASQ]}{\mathrm{d}t} = k_{+7}[AST^\ddagger] + k_{-11}[ASQT] - k_{+11}[ASQ][T] \tag{39}$$

$$\frac{\mathrm{d}[ASQT]}{\mathrm{d}t} = k_{+11}[ASQ][T] + k_{-12}[ASQT^\dagger] - k_{-11}[ASQT] - k_{+12}[ASQT] \tag{40}$$

$$\frac{\mathrm{d}[ASQT^\dagger]}{\mathrm{d}t} = k_{+12}[ASQT] + k_{-13}[ASQT^\ddagger] - k_{-12}[ASQT^\dagger] - k_{+13}[ASQT] \tag{41}$$

$$\frac{\mathrm{d}[ASQT^\ddagger]}{\mathrm{d}t} = k_{+13}[ASQT^\dagger] - k_{-13}[ASQT^\ddagger] - k_{+14}[ASQT] \tag{42}$$

$$\frac{\mathrm{d}[ASTQ]}{\mathrm{d}t} = k_{+14}[ASQT^\ddagger] - k_{+15}[ASTQ] \tag{43}$$

$$\frac{\mathrm{d}[ASTQ^\dagger]}{\mathrm{d}t} = k_{+15}[ASTQ] - k_{+16}[ASTQ] \tag{44}$$

$$\frac{\mathrm{d}[Q]}{\mathrm{d}t} = k_{+16}[ASTQ] \tag{45}$$

Supplementary Equations 3.

14

To examine the time-dependent concentration changes of reactants, intermediates and products over a given time interval, the system of ODEs is numerically integrated using the deterministic LSODA (17) algorithm of the ODEPACK library (18) within the Copasi package (19). LSODA stands for Livermore Solver for Ordinary Differential Equations and solves stiff and non-stiff systems of explicitly given ODEs. It starts using the non-stiff Adams integration method before dynamically deciding whether to switch to a non-stiff approach based on backward differentiation formula (BDF) for dense or banded Jacobians. Resulting linear systems are then solved by Factor-solve approach with LU factorization. For all time course simulations, relative and absolute tolerance is set to 10^{-6} and 10^{-12}, respectively. The maximum number of internal steps is fixed at 10^4, the option to integrate the reduced model is switched off. LSODA is a fast and reliable algorithm and the solution for a 432000 sec (4 d) time course of the described ODE systems with 10 or 13 ODEs and 20 or 29 parameters for the dissociative and the associative models, respectively, can be obtained within a few seconds on a MacBook Pro with 2.66 GHz Intel Core 2 Duo processor and 8 GB 1067 MHz DDR3 RAM, running Copasi 4.11 (Build 60, 64 Bit version).

Time of half-maximal target knockdown ($t_{1/2}$)

$t_{1/2}$ is defined as the time of half-maximal target knockdown, where target concentration $[T]t_{1/2} = [T]_0/2$, starting with basal target concentration $[T]_0$ at the time of siRNA administration. It is used as a contracted measure of time-resolved target knockdown to be able to relate model behaviour with two variables, i.e. basal target level and initial siRNA concentration in 3D-plots.

Computation of IC_{50} values from models by parameter optimisation

In case of models, IC_{50} values can be either extracted from dose-response curves relating the initial siRNA concentration in copies/cell to target gene activity in percent after 24 h time course simulation. A faster way of calculating a large number of IC_{50} for different initial conditions is via parameter optimisation algorithm. Here, the free parameter IC_{50} is set as the initial siRNA concentration $[siRNA]_0$ that minimises the expression $|[target]_{t=24h}$ (%) - 50%| while all other parameters are kept fixed during a 24h time course simulation. A simple and robust iterative algorithm (downhill simplex algorithm (20)) is used to solve the optimisation problem for a large number of initial conditions. In the few cases (< 1%), when no convergence was reached in reasonable computation time, the optimisation was repeated using a slower heuristic method (i.e. a genetic algorithm (21-24)).

Sensitivity analysis

The sensitivity analysis describes how small deviations of specific model parameters change the overall behaviour of the model. In this regard the analysis is closely related to Metabolic Control Analysis (MCA) (25,26). However, MCA looks into steady state properties of biochemical networks, whereas this analysis is designed to comprehend the time-resolved properties of the modelled RNAi pathway. The global response of the system (i.e. target knockdown efficacy 24h post siRNA transfection) to perturbations from the network structure given its parameters (i.e. kinetic rate constants, initial concentrations of reactants and reaction volumes) is analysed. Sensitivity coefficients ε_k^i quantify the sensitivity of a 24 h time course of target concentration to small parameter changes S_i as a function of basal target concentration $[T]_0 = C_k$. The relative target concentration (in %) during the time course is differentiated with respect to the investigated parameters S_i using finite differences with delta factor 0.001 and delta minimum

15

10^{-12}. Investigated parameters S_i are kinetic rate constants, initial concentrations of reactants, as well as, cytoplasm volume. Sensitivity coefficients are normalised between -1 and 1.

The sensitivity analysis yields important information's about specific parameter values. If a parameter is found not to affect the system considerably, a rough guess of its value may be sufficient. However, if on the other hand a parameter influences the behaviour of the model substantively, steps must be taken to determine its value more accurately. Furthermore, sensitivity analysis gives information about which parameters should be changed (or kept as constant as possible) to achieve a specific effect (or avoid a specific effect). Additionally, robustness of system against external influences, i.e. transfection of siRNA, target levels, target metabolism etc. can be determined via sensitivity analyses.

Given the results for the associative model in Supplementary Figure S6 for typical target concentrations of 1–100 copies/cell, increase of siRNA concentration does not lead to better target knock-down efficacy. Thus, it is not worth to risk off-target and side effects associated with transfection of high amounts of siRNA. The dissociative model is sensitive to changes in rate constants of binary complex formation (k_{+2}, k_{-2}, k_{+3}, and k_{-3}), as well as ternary complex formation (k_{+4}, k_{-4}, k_{+5}, k_{-5}, and k_{+6}). These parameters limit knockdown efficacy for low target concentrations up to 1,000 or 2,000 copies/cell (for 30 or 300 siRNAs/cell, respectively). At higher target concentrations the knockdown efficacy is practically zero (no target knock-down after 24 h). Thus, changes of any rate constant will not lead to rescue of the knockdown efficacy (sensitivity is zero as shown by the green colour in Supplement Figure S6 for all the parameters). Just before this breakdown in efficacy occurs, the system becomes sensitive to k_{+10} (i.e. product release), which can be identified as the limiting step / bottleneck for knock-down efficacy when increasing target concentration. In comparing the two models, it becomes evident the associative model is far less sensitive to changes of binary or ternary complex formation at low target concentrations. In contrast to the dissociative model, the knock-down efficacy is sustained even for higher target concentrations. Here, product release does not become the limiting step. However, association/dissociation of target into the reaction complex (i.e. quaternary complex formation; k_{+11}, k_{-11}, k_{+12}, k_{-12} and k_{+13}) might eventually limit efficacy.

Supplementary References

1.	Deerberg, A., Willkomm, S. and Restle, T. (2013) Minimal mechanistic model of siRNA-dependent target RNA slicing by recombinant human Argonaute 2 protein. *Proc Natl Acad Sci U S A*, **110**, 17850-17855.
2.	Kati, W.M., Johnson, K.A., Jerva, L.F. and Anderson, K.S. (1992) Mechanism and fidelity of HIV reverse transcriptase. *J Biol Chem*, **267**, 25988-25997.
3.	Puck, T.T., Marcus, P.I. and Cieciura, S.J. (1956) Clonal growth of mammalian cells in vitro; growth characteristics of colonies from single HeLa cells with and without a feeder layer. *J Exp Med*, **103**, 273-283.
4.	Cohen, L.S. and Studzinski, G.P. (1967) Correlation between cell enlargement and nucleic acid and protein content of HeLa cells in unbalanced growth produced by inhibitors of DNA synthesis. *Journal of Cellular Physiology*, **69**, 331-339.
5.	Lim, L.P., Lau, N.C., Weinstein, E.G., Abdelhakim, A., Yekta, S., Rhoades, M.W., Burge, C.B. and Bartel, D.P. (2003) The microRNAs of Caenorhabditis elegans. *Genes Dev*, **17**, 991-1008.
6.	Fujioka, A., Terai, K., Itoh, R.E., Aoki, K., Nakamura, T., Kuroda, S., Nishida, E. and Matsuda, M. (2006) Dynamics of the Ras/ERK MAPK cascade as monitored by

fluorescent probes. *J Biol Chem*, **281**, 8917-8926.

7.   Moran, U., Phillips, R. and Milo, R. (2010) SnapShot: key numbers in biology. *Cell*, **141**, 1262-1262 e1261.

8.   Janas, M.M., Wang, B., Harris, A.S., Aguiar, M., Shaffer, J.M., Subrahmanyam, Y.V., Behlke, M.A., Wucherpfennig, K.W., Gygi, S.P., Gagnon, E. *et al.* (2012) Alternative RISC assembly: binding and repression of microRNA-mRNA duplexes by human Ago proteins. *Rna*, **18**, 2041-2055.

9.   Wang, D., Zhang, Z., O'Loughlin, E., Lee, T., Houel, S., O'Carroll, D., Tarakhovsky, A., Ahn, N.G. and Yi, R. (2012) Quantitative functions of Argonaute proteins in mammalian development. *Genes Dev*, **26**, 693-704.

10. Velculescu, V.E., Madden, S.L., Zhang, L., Lash, A.E., Yu, J., Rago, C., Lal, A., Wang, C.J., Beaudry, G.A., Ciriello, K.M. *et al.* (1999) Analysis of human transcriptomes. *Nat Genet*, **23**, 387-388.

11. Wilsbacher, L.D., Yamazaki, S., Herzog, E.D., Song, E.J., Radcliffe, L.A., Abe, M., Block, G., Spitznagel, E., Menaker, M. and Takahashi, J.S. (2002) Photic and circadian expression of luciferase in mPeriod1-luc transgenic mice invivo. *Proc Natl Acad Sci U S A*, **99**, 489-494.

12. Yang, E., van Nimwegen, E., Zavolan, M., Rajewsky, N., Schroeder, M., Magnasco, M. and Darnell, J.E., Jr. (2003) Decay rates of human mRNAs: correlation with functional characteristics and sequence attributes. *Genome Res*, **13**, 1863-1872.

13. Detzer, A. (2010), Small interfering RNA (siRNA): Zelluläre Einschleusung und Wirkmechanismen, PhD thesis, University of Lübeck, Lübeck, Germany.

14. Lee, E.J., Baek, M., Gusev, Y., Brackett, D.J., Nuovo, G.J. and Schmittgen, T.D. (2008) Systematic evaluation of microRNA processing patterns in tissues, cell lines, and tumors. *Rna*, **14**, 35-42.

15. Laufer, S.D. (2008), Quantitative Untersuchung der Aufnahme und des biologischen Effekts von oligomeren Nukleinsaurewirkstoffen nach Peptid-vermitteltem Transport in Säugerzellen, PhD thesis, University of Lübeck, Lübeck, Germany.

16. Laufer, S.D., Detzer, A., Sczakiel, G. and Restle, T. (2010) In Erdmann, V. A., Barciszewski, J. (ed.), *RNA Technologies and Their Applications*. Springer, pp. 29-58.

17. Petzold, L. (1983) Automatic Selection of Methods for Solving Stiff and Nonstiff Systems of Ordinary Differential-Equations. *SIAM Journal on Scientific and Statistical Computing*, **4**, 136-148.

18. Hindmarsh, A. (1983) In RS, S. (ed.), *IMACS Transactions on Scientific Computation In IMACS Transactions on Scientific Computation, Vol. 1*. 1 ed. Scientific Computing, Amsterdam, North-Holland, pp. 55-64.

19. Hoops, S., Sahle, S., Gauges, R., Lee, C., Pahle, J., Simus, N., Singhal, M., Xu, L., Mendes, P. and Kummer, U. (2006) COPASI--a COmplex PAthway SImulator. *Bioinformatics*, **22**, 3067-3074.

20. Nelder, J.A. and Mead, R. (1965) A Simplex-Method for Function Minimization. *Comput J*, **7**, 308-313.

21. Bäck, T. and Schwefel, H.-P. (1993) An Overview of Evolutionary Algorithms for Parameter Optimization. *Evolutionary Computation*, **1**, 1-23.

22. Michalewicz, Z. (1996) *Genetic algorithms + data structures = evolution programs*. 3 ed. Springer Verlag.

23. Bäck, T., Fogel, D.B. and Michalewicz, Z. (1997) *Handbook of Evolutionary Computation*. IOP Publishing Ltd. Bristol, UK, UK.

24. Mitchell, M. (1998) *An Introduction to Genetic Algorithms (Complex Adaptive Systems)*. The MIT Press.

25. Kacser, H. and Burns, J.A. (1973) The control of flux. *Symp Soc Exp Biol*, **27**, 65-104.

26. Heinrich, R. and Rapoport, T.A. (1974) A linear steady-state treatment of enzymatic chains. General properties, control and effector strength. *Eur J Biochem*, **42**, 89-95.